

# Matrix product states and the nonabelian rotor model

Ashley Milsted\*

Leibniz Universität Hannover, Institute of Theoretical Physics, Appelstrasse 2, D-30167 Hannover, Germany

(Dated: June 14, 2021)

We use uniform matrix product states (MPS) to study the (1+1)D  $O(2)$  and  $O(4)$  rotor models, which are equivalent to the Kogut-Susskind formulation of matter-free nonabelian lattice gauge theory on a “hawaiian earring” graph for  $U(1)$  and  $SU(2)$ , respectively. Applying tangent space methods to obtain ground states and determine the mass gap and the  $\beta$  function, we find excellent agreement with known results, locating the BKT transition for  $O(2)$  and successfully entering the asymptotic weak-coupling regime for  $O(4)$ . To obtain a finite local Hilbert space, we truncate in the space of generalized Fourier modes of the gauge group, comparing the effects of different cutoff values. We find that higher modes become important in the crossover and weak-coupling regimes of the nonabelian theory, where entanglement also suddenly increases. This could have important consequences for TNS studies of Yang-Mills on higher dimensional graphs.

## I. INTRODUCTION

Nonabelian gauge theories describe the interactions responsible for most of the matter we experience in our everyday lives. In particular, they explain the hadrons — bound states of quarks — which include neutrons and protons among their most famous examples [1]. Curiously, the quarks inside hadrons behave as free particles for the purposes of high-energy scattering (asymptotic freedom), yet they are never observed in isolation (confinement [2]). These properties are also present in matter-free nonabelian gauge theory (pure Yang-Mills theory). This apparently simple theory, despite its huge symmetry group of local gauge transformations, resists exact solution and must so far be approached with approximate methods such as perturbation theory and numerical tools such as Monte Carlo sampling [3], albeit with convincing successes, such as the determination of Hadron masses using lattice simulations [4].

Monte Carlo techniques are also extremely useful in condensed matter physics and advances have benefited both fields. However, in recent decades new, highly general techniques have arisen in condensed matter and quantum information that open up whole new avenues of numerical investigation. These techniques exploit Tensor Network States (TNS) [5], which efficiently represent many-body states with limited *entanglement*. The best-known example is the density-matrix renormalization group (DMRG) [6], which can be viewed [7] as a variational algorithm applied to one-dimensional TNS, also known as Matrix Product States (MPS) [8]. These methods are inherently free of the sign problem that plagues Monte Carlo sampling [9] and offer themselves naturally to simulation of real-time dynamics.

In the last years, as TNS techniques have advanced (higher dimensions, more sophisticated networks, improved numerical tools) [10], efforts have increased to transfer their successes in condensed matter to quantum

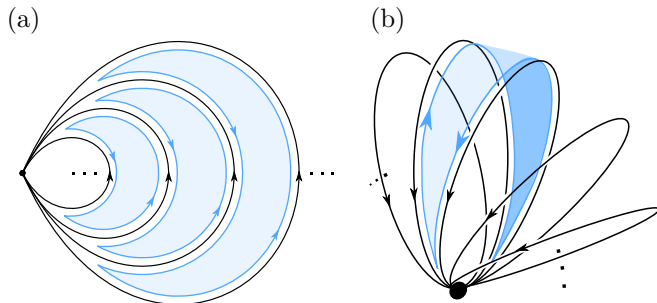


Figure 1. Illustration of lattice gauge theory (a) on a “hawaiian earring” and (b) the same theory visualized differently as living on the surface of a 3D object. The Hamiltonian is the Kogut-Susskind [29] formulation of lattice gauge theory for a gauge group  $G$  — example plaquette operators are shown in blue. The Hilbert space  $\mathcal{H}$  (including non-physical states) is made up of systems living on the (black) edges  $\mathcal{H}_{\text{edge}} \cong L^2(G)$ . For the gauge groups  $G \cong U(1)$  and  $G \cong SU(2)$  this model is equivalent to the (1+1)-dimensional quantum rotor model [30] for the rotation groups  $O(2)$  and  $O(4)$ , respectively.

field theory, particularly with an eye toward nonabelian gauge theory. Important steps in this direction include ground state, real-time, and finite-temperature simulations of  $\phi^4$  theory [11, 12], the Schwinger model [13–16],  $SU(2)$  gauge theory with matter [17] in (1+1)D, and quasi-one-dimensional abelian gauge theories [18], all using MPS or DMRG, as well as proposals for representing lattice gauge theory states in higher dimensions, with a view toward numerics as well as analytics [19–23]. The tensor renormalization group (TRG) algorithm [24] has also been applied to  $\phi^4$  theory [25], the Schwinger model [26], and the  $O(2)$  and  $O(3)$  models [27, 28].

## A. This work

Here we present an MPS study of the  $O(2)$  and  $O(4)$  quantum rotor models in 1 + 1D, which are equivalent, respectively, to the  $U(1)$  and  $SU(2)$  principal chiral field

\* ashley.milsted@itp.uni-hannover.de

(PCF) models. The PCF model is in turn equivalent to a pure lattice gauge theory on a “hawaiian earring” graph in the Kogut-Susskind formulation (see Figure 1), insofar as we do not restrict to gauge-invariant states.

The Hamiltonians possess a global gauge-group symmetry rather than a local gauge symmetry, but nevertheless have a lot in common with Yang-Mills on more sophisticated graphs. Most importantly, the  $O(N > 2)$  models are known to possess a single, gapped phase ending at the weak-coupling limit  $g \rightarrow 0$  [30]. This is also observed in simulations of  $(3 + 1)$ D nonabelian lattice gauge theory, in which the gapped phase is confining [2]. In contrast, the  $O(2)$  model has a phase transition (of Berezinskii-Kosterlitz-Thouless (BKT) type [31]) at finite coupling, transitioning into a deconfined, gapless phase at weaker couplings.

The continuum limit of the rotor models, the so-called  $O(N)$  nonlinear sigma model [30], can be solved using the Bethe ansatz for  $N > 2$  making the lattice weak-coupling scaling of the mass gap computable [32]. The  $O(N)$  model has also been thoroughly investigated using strong-coupling expansions [33, 34], which operate on the same  $1 + 1$ D Hamiltonian model we study here, as well as high-temperature expansions (for example [35]) and Monte Carlo numerics ([36–39] is an incomplete selection) applied to the 2D classical  $O(N)$  model. Lanczos diagonalization with finite-size-scaling has also been used [40]. In this work, we use uniform MPS to represent infinite, translation invariant states, applying the nonlinear conjugate gradient method [12] to obtain ground states and the MPS tangent space as an ansatz for low energy excitations [41, 42], determining the mass gap and the  $\beta$  function at finite couplings and thus obtaining the phase diagram.

## II. THE MODEL

### A. Kogut-Susskind Hamiltonian

The Kogut-Susskind Hamiltonian [29] on the “hawaiian earring” graph is given by

$$H_{\text{KS}}(g) = \frac{\sqrt{\eta}g^2}{2a} \sum_{k=-\infty}^{+\infty} E_k^2 - \frac{2\sqrt{\eta}}{g^2a} \sum_{k=-\infty}^{+\infty} \text{Re}(\text{tr}(u_k u_{k+1}^\dagger)), \quad (1)$$

where  $g$  is the coupling,  $a$  the lattice spacing, and  $\eta$  an anisotropy parameter required to ensure the renormalized theory is Lorentz-invariant in the continuum limit [43]. The Hilbert space is the tensor product of spaces

$$\mathcal{H}_k = L^2(G)$$

assigned to each edge  $e$  in the graph and  $G$  is the gauge group. We define  $\lambda_\alpha$  to be the Hermitian generators of  $G$  (for  $SU(2)$  these are the Pauli matrices  $\lambda_\alpha = \frac{1}{2}\sigma_\alpha$  with  $\alpha = 1, 2, 3$ , for  $U(1)$  there is only one  $\lambda = 1$ ). The

operator

$$E_k^2 = \sum_{\alpha} E_{\alpha,k}^2$$

is the quadratic Casimir operator representing the kinetic energy within the gauge group at edge  $k$ . The  $E_\alpha$  represent the infinitesimal group action

$$E_\alpha := \partial_\epsilon L_{e^{i\epsilon\lambda_\alpha}}|_{\epsilon=0},$$

where  $L_x$  implements rotations from the left, acting on a “position” basis as

$$L_x|v\rangle = |xv\rangle$$

for  $x, v \in G$ . The  $u_{ij}$  are gauge group position operators defined as

$$u_{ij}|v\rangle = t(v)_{ij}|v\rangle,$$

with  $t(v)$  an irrep of  $G$  (we choose  $e^{i\theta}$  for  $U(1)$  and the spin-half representation for  $SU(2)$ ). This results in the commutator

$$[E_\alpha, u_{ij}] = \sum_{j'} \lambda_{\alpha,ij'} u_{j'j}.$$

### B. Quantum Rotor Hamiltonian

The model (1) is known to be equivalent to a chain of coupled  $O(N)$  rotors (see e.g. [43]), given by

$$H_{\text{R}}(\tilde{g}) = \frac{\sqrt{\eta}\tilde{g}}{2a} \sum_{k=-\infty}^{+\infty} \mathbf{J}_k^2 - \frac{\sqrt{\eta}}{\tilde{g}a} \sum_{k=-\infty}^{+\infty} \mathbf{n}_k \cdot \mathbf{n}_{k+1}, \quad (2)$$

where  $\mathbf{n}_k$  is a  $N$ -dimensional unit vector representing the  $k$ th rotor and  $\mathbf{J}_k^2$  is the rotor kinetic energy. The normalization of  $\mathbf{J}^2$  is chosen to match [33]. The Hamiltonian (2) is manifestly invariant under a global  $O(N)$  symmetry. The relations which underlie  $H_{\text{KS}} = H_{\text{R}}$  are given in Table I.

$H_{\text{R}}, O(N)$	$H_{\text{KS}}, G \cong U(1)$	$H_{\text{KS}}, G \cong SU(2)$
$N$	2	4
$\tilde{g}$	$g^2/\sqrt{2}$	$g^2/4$
$\mathbf{J}^2$	$E^2$	$4E^2$
$\mathbf{n}_\mu$	$(\text{Re}(u), \text{Im}(u))_\mu$	$-i \text{tr}(\lambda_\mu u)$
	$\mu = 1, 2$	$\mu = 0 \dots 3, \lambda_0 = \frac{1}{2}\mathbb{I}$

Table I. This table shows how quantities in the rotor model (2) must be set to obtain equivalence to the Kogut-Susskind model (1) for the gauge groups  $G \cong U(1)$  and  $G \cong SU(2)$ .

The continuous position basis  $|v\rangle$  does not lend itself to use with MPS numerics, for which we require a discrete, finite basis  $\cong \mathbb{C}^d$ . Instead we make use of the generalized Fourier basis given by the Peter-Weyl theorem [44], in

which the matrix elements of the irreducible representations (irreps) of a compact Lie group  $G$  label generalized Fourier modes  $|ij\rangle_l$  (the matrix element  $i, j$  of irrep  $l$ ). The kinetic term  $E^2$  is diagonal in this basis, with

$$E^2|ij\rangle_l = l(l+1)|ij\rangle_l, \quad l \in \frac{1}{2}\mathbb{Z}^*$$

for  $SU(2)$  and

$$E^2|n\rangle = n^2|n\rangle, \quad n \in \mathbb{Z}$$

for  $U(1)$ . In the strong coupling regime  $g^2 \gg 1$ , the  $E^2$  term strongly penalizes higher irreps, so we can neglect them to good approximation at larger  $g^2$ , expecting them to become more relevant as we near weak coupling. Importantly, truncating the basis at a certain irrep level (Fourier mode) does not prevent representation of states invariant under the global gauge-group symmetry (since rotations do not mix irreps).

### III. NUMERICAL METHODS

The uniform MPS variational class consists of states

$$|\Psi(A)\rangle = \sum_{s=1}^d v_L^\dagger \left[ \prod_{k=-M}^{+M} A^{s_k} \right] v_R |s_{-M} \dots s_0 \dots s_{+M}\rangle,$$

where  $A^s$  is a  $D \times D$  matrix and  $d$  the dimension of the chosen local basis and we make the chain length infinite:  $M \rightarrow \infty$ . For a given basis element  $\mathbf{s} = (s_{-M}, \dots, s_{+M})$ , the matrix product in square brackets determines the value of  $\langle s_{-M} \dots s_0 \dots s_{+M} | \Psi(A) \rangle$ , hence the name ‘‘matrix product states.’’ Two key features of MPS are the efficiency with which quantities such as expectation values of local operators and correlation functions can be computed (requiring  $\mathcal{O}(D^3)$  multiplications), and the fact that the restriction to MPS form serves only to limit the amount of entanglement that can be present in the state. The dimension  $D$  is called the bond dimension and serves to control the degree of spatial correlations, placing an upper bound  $S \leq \log D$  on the entanglement entropy, for example. For more background, see for example [5].

To make the limit  $M \rightarrow \infty$  behave appropriately, we require  $A$  such that the *transfer operator*

$$E := \sum_s A^s \otimes \overline{A^s}$$

has spectral radius  $\rho(E) = 1$  with a unique eigenvalue of largest magnitude (injectivity) equal to one. With this condition, the boundary vectors  $v_L$  and  $v_R$  drop out of all relevant calculations and  $\langle \Psi(A) | \Psi(A) \rangle = 1$ . For more details on using infinite, uniform MPS, see [10].

We set  $d$  to accommodate the dimensions of all Fourier modes up to a cutoff. With  $U(1)$  all irreps are one-dimensional and we may label Fourier modes as  $n \in \mathbb{Z}$ , so that a cutoff is given by  $|n| \leq n_{\max}$  and

$$d = 2n_{\max} + 1.$$

For  $SU(2)$  we must set

$$d = \sum_{l=0}^{l_{\max}} \dim(V_l)^2 = \sum_{l=0}^{l_{\max}} (2l+1)^2,$$

with  $l = 0, \frac{1}{2}, 1, \frac{3}{2}, \dots$ .

In this study, we use values of  $n_{\max}$  up to 10 and  $l_{\max}$  up to 2. The former requires  $d = 21$ , while the latter implies  $d = 55$ , which is unusually high for MPS numerics. In the algorithms of [12, 41, 45] the cost of computations involving nearest-neighbor operators, such as the potential term  $u_e u_{e+1}^\dagger$ , scales as  $\mathcal{O}(d^4)$ . We reduce this to  $\mathcal{O}(d^2 m)$ , where  $m$  is the number of terms in the tensor product decomposition, by implementing them as two-site matrix product operators [7] of dimension  $m$ , where  $m \leq 4$  for our purposes. We further accelerate our implementation by computing the iterands of iterative parts using general purpose graphics processing units (GPGPU’s) [46].

With these optimizations, we apply the nonlinear conjugate gradient (CG) method to obtain ground states [12], with the time-dependent variational principle [45] used in a pre-optimization step to provide good starting points for the CG algorithm. We converge all states up to  $\|P_{T(A)} H |\Psi(A)\rangle\| \leq 10^{-8}$ , where  $P_{T(A)}$  projects the energy gradient vector onto the MPS tangent space at  $|\Psi(A)\rangle$ . We then obtain low-lying excited states using the methods of [41], always operating directly in the space of infinite, uniform MPS. All MPS algorithms used here are implemented as part of the open source *evoMPS* project [47].

## IV. RESULTS

### A. Phases observed

Since our choice of truncated basis is most appropriate at strong coupling, we study the system starting at  $1/\tilde{g} \rightarrow 0$  and then approach weak-coupling as far as possible, whilst maintaining accuracy. We find, for both the  $O(2)$  and the  $O(4)$  rotor, that the MPS approximate ground state breaks the global  $O(N)$  symmetry for  $1/\tilde{g} < 1/\tilde{g}_{\text{SB}}$  for constant, finite  $D$ . The symmetry-breaking, for the values of  $D$  in use, is confined to a relatively narrow region of parameter space. Since the breaking of a continuous symmetry is forbidden by the Mermin-Wagner theorem [48], this must be a symptom of finite-entanglement effects [49]: The bond dimension needed to accurately represent the symmetric state must suddenly grow as we approach weak coupling.

The  $O(2)$  rotor is known to possess a gapless phase at weak coupling, characterized by algebraically decaying correlations, such that the correlation length is infinite [30]. As defined above, a uniform MPS would require  $D \rightarrow \infty$  to accurately represent such a ground state, thus explaining nonphysical symmetry-breaking at finite

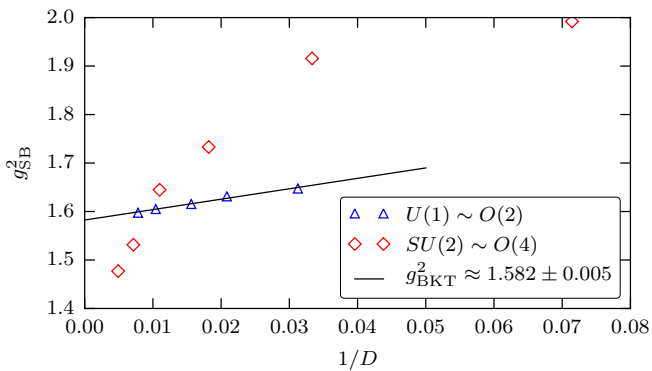


Figure 2. The location  $g_{\text{SB}}^2$  of MPS ground state symmetry breaking (SB) as a function of the bond dimension  $D$ . We plot the Kogut-Susskind coupling  $g_{\text{SB}}^2$  rather than  $\tilde{g}_{\text{SB}}$  to aid comparison. Values of  $g_{\text{SB}}^2$  were found using bisection up to a precision in  $g^{-2}$  of  $\pm 0.005$ . For  $U(1) \sim O(2)$ ,  $g_{\text{SB}}^2$  tends toward a finite value. This value should correspond to the location of the BKT transition [30]. In terms of the  $O(2)$  rotor parameter the fit gives  $\tilde{g}_{\text{BKT}} = 1.119 \pm 0.004$ . For  $SU(2) \sim O(4)$ , the transition does not converge for the data available. This is consistent with it occurring at  $g = \tilde{g} = 0$ .

$D$ . The existence of a phase transition at finite  $\tilde{g}$  also explains the narrowness of the region where symmetry-breaking begins. We expect the symmetry-breaking location  $\tilde{g}_{\text{SB}}(D)$  to converge to the location of the phase transition as  $D \rightarrow \infty$  and indeed this convergence can be seen in Figure 2, where the extrapolated transition point  $\tilde{g} = 1.119 \pm 0.004$  agrees well with a known estimate from strong-coupling expansions of the mass gap  $\tilde{g} \approx 1.12$  [33] and less well with an estimate  $\tilde{g} \approx 1.05$  based on Padé approximations of  $\beta$ -functions from strong-coupling expansions [34], as well as a number of other methods [50] that indicate  $\tilde{g} \approx 1.00$  (the parameter given in these studies is usually  $x = 2/\tilde{g}^2$ ). It is worth noting that estimating the transition point of a BKT transition is notoriously difficult due to the exponential scaling of the mass gap near the transition [31] and it is possible that our estimate would shift given data at larger bond dimensions, or by the use of more reliable indicators than the onset of nonphysical symmetry-breaking. An accurate determination of  $\tilde{g}_{\text{BKT}}$  is, however, beyond the scope of this work.

Despite the impossibility of representing the ground state precisely in the gapless phase at weak coupling, the scaling of von Neumann entropy and correlation length in MPS ground states with a range of finite  $D$  can be used to estimate the central charge  $c$  of the conformal field theory (CFT) describing the phase [51, 52]. We fit data for  $D = 22, 28, 34, \dots, 80$  at  $1/(\tilde{g}\sqrt{2}) = 0.75, 0.8, 0.85, 0.9$  and find  $c = 0.992 \pm 0.009$ , matching the known result of  $c = 1$  for the 2D classical XY model [53], which is identical with the classical  $O(2)$  rotor.

We now turn to the  $O(4)$  rotor, which is known to exist in a single, gapped phase down to the weak-coupling limit  $\tilde{g} \rightarrow 0$  [30]. Here, we expect our choice of basis to become

increasingly bad as we approach weak-coupling, due to the occupation of higher Fourier modes. We also expect greater entanglement in the exact ground state as the potential term, coupling nearest-neighbor edges, begins to dominate, and the lattice correlation length grows. This is not enough, however, to explain the very sudden occurrence of nonphysical symmetry-breaking. This is likely due to the “crossover” phenomenon, a property of the  $O(N > 2)$  models and of nonabelian gauge theories, referring to persistence of strong-coupling behavior up to a certain region of parameter space, where weak-coupling behavior rapidly takes over. Despite the sudden onset of the weak-coupling regime, we still expect the nonphysical symmetry-breaking transition to disappear as  $D \rightarrow \infty$ , as we indeed observe in Figure 2.

## B. Mass gap

Our next source of information is the mass gap. Here, we can directly compare our results with the results of 8th-order and 6th-order strong-coupling series expansions (SCE) for the  $O(2)$  and  $O(4)$  models, respectively [33]. We find excellent agreement for both models up to the vicinity of the  $O(2)$  phase transition and the  $O(4)$  crossover region. Moving closer, Figure 3 shows that the mass gap descends toward zero at a finite coupling for  $O(2)$ , whereas for  $O(4)$  the log-linear plot shows linear behavior, indicating a finite mass gap for all finite couplings. For comparison, we plot the exact asymptotic weak-coupling scaling for  $O(4)$  [32], taking into account speed-of-light renormalization effects due to the stark space-time asymmetry of the Hamiltonian discretization [43]. We find very good agreement with the weak-coupling prediction, showing that we are successfully entering the asymptotic scaling regime, although we also see from the plot that finite entanglement effects start to limit the accuracy (the  $D = 140$  curve remains accurate for longer than the  $D = 91$  curve for  $l_{\text{max}} = 2$ ), as indeed does the Fourier mode truncation (the  $l_{\text{max}} = 2$  curve is more accurate than the  $l_{\text{max}} = 3/2$  curve for  $D = 140$ ).

In the  $O(4)$  case it is also interesting to note that, holding the Fourier cutoff at  $l \leq 2$ , increasing the bond dimension appears to interpolate between the SCE result and the weak-coupling result. The effect is even clearer when more values of  $D$  are considered. This makes sense if we recall that the SCE for the mass gap perturbs the  $\tilde{g} \rightarrow \infty$  ground state and first excited state, both product states without entanglement in the Fourier basis, by repeatedly applying the nearest-neighbor term in the Hamiltonian up to some order [29, 33]. The higher the order, the less local the correlations introduced into the states will be. In the same way, raising the bond dimension of an MPS ground state utilizing the Fourier basis allows longer-range correlations to be represented. In this sense, our MPS methods and SCE’s are very similar techniques, and it is not surprising that the MPS results at smaller bond dimensions match low-order SCE results well.

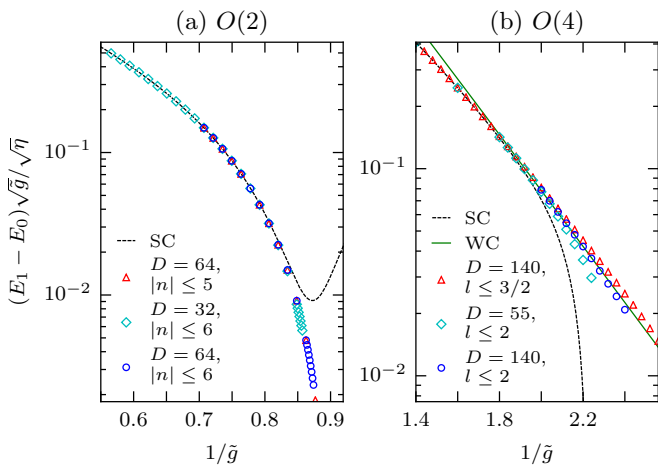


Figure 3. The MPS mass gap for (a) the  $O(2)$  rotor and (b) the  $O(4)$  rotor for bond dimensions  $D$  and Fourier cutoffs in  $|n|$  and  $l$  respectively. The strong coupling expansion of [33] is shown (SC), as is the weak coupling result (WC) for the  $O(4)$  case, which is known exactly [32]. In (b), the curves are adjusted by an anisotropy parameter  $\sqrt{\eta}$  to account for the renormalization of the speed of light [43] (for  $O(2)$ ,  $\eta$  is set to one). Near the phase transition for  $O(2)$ , and as we enter the weak coupling regime for  $O(4)$ , finite entanglement effects and, for  $O(4)$ , Fourier cutoff effects become important.

Using similar reasoning, we can understand why the SCE results and the lower- $D$  MPS results *underestimate* the mass gap in the  $O(4)$  weak-coupling regime. Given that the ground state in this region consists of highly non-local structures (Wilson loop excitations of various sizes) [29], limiting the order of the SCE or restricting the amount of entanglement in the MPS should both work against achieving these low-energy configurations, resulting in an overestimation of the ground state energy. Indeed, we observe significant differences on the order of  $10^{-2}$  in the ground state energy with  $D$  as we enter the crossover regime. Assuming the first excitation is represented relatively accurately, this explains the underestimation of the gap.

We note here that using a symmetric tensor network ansatz [54] might significantly extend the range of accessible effective bond dimensions and so enable further penetration into the  $O(4)$  weak-coupling regime, although it would not allow access to the lowest-lying excitations of the  $O(4)$  model, which break the  $O(4)$  symmetry. For a model with truly local gauge symmetry, methods such as that of [16] are required.

### C. Beta functions

Using the mass gap and its first derivative in the coupling, one can calculate (see, for example [33]) the  $\beta$  func-

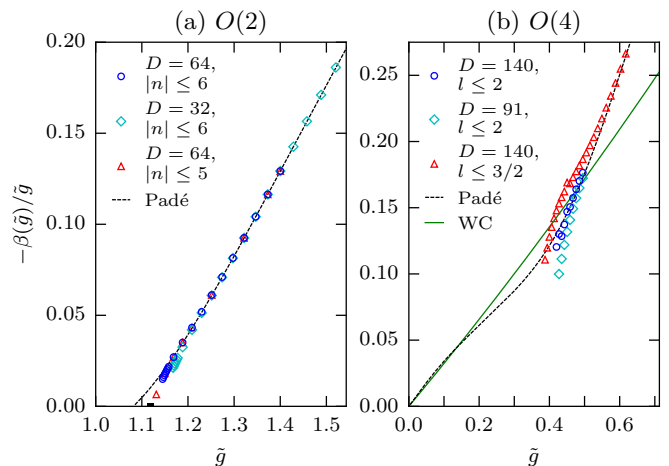


Figure 4. Beta functions determined from the MPS mass gap for (a) the  $O(2)$  rotor and (b) the  $O(4)$  rotor, together with a Padé approximant based on a strong-coupling expansion and the weak coupling result (WC) for the nonabelian case [33]. The estimate  $\tilde{g}_{\text{BKT}}$  from Figure 2 of the location of the  $O(2)$  phase transition is marked in (a) using a black rectangle. For  $O(4)$  it is clear from the  $D = 140$ ,  $l_{\text{max}} = 3/2$  curve that the numerical results begin to qualitatively follow the weak coupling behavior. However, there are clearly systematic errors present. This is expected because the beta function involves the numerical derivative of the mass gap, making it sensitive to small inaccuracies due to finite entanglement and Fourier mode truncation.

tion as

$$-\beta(\tilde{g})/\tilde{g} = \left(1 - \frac{4}{\tilde{g}^2} \frac{F'(\tilde{g})}{F(\tilde{g})}\right)^{-1},$$

where  $F(\tilde{g}) = 2a(E_1(\tilde{g}) - E_0(\tilde{g}))/\tilde{g}$ . Using finite-differences to compute  $F'$ , we may compute  $\beta$  functions from our mass gap results.

It is also possible to use an SCE for the mass gap to construct a Padé approximant for the  $\beta$  function. Furthermore, the  $O(N > 2)$  weak-coupling behavior of  $\beta(\tilde{g})$  is known from perturbation theory to be

$$-\beta(\tilde{g}) = (N-2)\frac{\tilde{g}^2}{2\pi} + (N-2)\frac{\tilde{g}^3}{4\pi^2},$$

allowing this information to be incorporated, resulting in an approximate  $\beta$  function for all couplings for the  $O(N > 2)$  rotor [33].

We compare the Padé approximants of [33] with our MPS results in Figure 4, observing excellent agreement at stronger couplings, with the numerical results deviating from the approximate curve as we near the phase transition. In the case of  $O(2)$ , the numerical data appears to predict a higher value for the phase transition location than the Padé approximant, in good agreement with our result from Figure 2. However, we also observe a shift in the results as the bond-dimension changes, with the higher- $D$  results corresponding to a smaller prediction for  $\tilde{g}_{\text{BKT}}$ . This supports the possibility mentioned in

the previous section that using higher bond-dimensions would result in a better correspondence with the majority of literature results.

The  $O(4)$  data ceases to follow the Padé curve as we enter the crossover region, but does not succeed in following the weak-coupling result accurately either. This is not unexpected, as both approximations are likely inaccurate in the crossover region. We do, however, see large variations with  $D$  and  $l_{\max}$ , particularly as we near the nonphysical symmetry-breaking transition. That errors are more visible for the  $\beta$  function than for the mass gap is expected since the numerical derivative amplifies small errors in the mass gap. We would need to reach higher bond dimensions and Fourier mode cutoffs to achieve accurate results further into the weak-coupling regime. A further way of reducing noise would be to compute the derivative  $F'(x)$  analytically from the MPS excited state.

## V. CONCLUDING REMARKS

We have shown that tensor network state (TNS) methods, in this case uniform matrix product states (MPS),

can successfully represent states of the nonabelian quantum rotor model into the weak-coupling regime. The finite local basis, achieved through Fourier-mode truncation successfully and efficiently captures strong-coupling physics, but becomes a more severe limitation at weak couplings where, additionally, the spatial entanglement grows substantially.

This is promising for TNS approaches to pure nonabelian gauge theory, which is believed to possess a very similar phase diagram to the  $O(N)$  rotor models and, on the “hawaiian earring” graph, is indeed equivalent to the rotor models studied here. Our study also shows that high spatial entanglement is a feature of the theory from the crossover region onward, into weak-coupling. This may pose a challenge for numerical approaches if it carries over to higher dimensional nonabelian lattice gauge theory, since large bond dimensions may be needed to access the asymptotic scaling regime.

The author would like to thank Tobias J. Osborne, Leander Fiedler, Courtney Brell, Karel Van Acoleyen and Kais Abdelkhalek for inspiring discussions. This work was supported by the ERC Grants QFTCMPS and SIQS and by the cluster of excellence EXC 201 Quantum Engineering and Space-Time Research.

- 
- [1] M. E. Peskin and D. V. Schroeder, *An Introduction To Quantum Field Theory* (Westview Press, 1995).
  - [2] J. Greensite, *An Introduction to the Confinement Problem*, Lecture Notes in Physics, Vol. 821 (Springer Berlin Heidelberg, Berlin, Heidelberg, 2011).
  - [3] M. Creutz, *Quarks, Gluons and Lattices* (Cambridge University Press, 1985).
  - [4] S. Dürr, Z. Fodor, J. Frison, C. Hoelbling, R. Hoffmann, S. D. Katz, S. Krieg, T. Kurth, L. Lellouch, T. Lippert, K. K. Szabo, and G. Vulvert, *Science* **322**, 1224 (2008).
  - [5] J. C. Bridgeman and C. T. Chubb, [arXiv:1603.03039](https://arxiv.org/abs/1603.03039) (2016).
  - [6] S. R. White, *Phys. Rev. Lett.* **69**, 2863 (1992).
  - [7] U. Schollwöck, *Ann. Phys.* **326**, 96 (2011).
  - [8] M. Fannes, B. Nachtergaele, and R. F. Werner, *Commun. Math. Phys.* 1965-1997 **144**, 443 (1992); S. Rommer and S. Östlund, *Phys. Rev. B* **55**, 2164 (1997); G. Vidal, *Phys. Rev. Lett.* **93**, 040502 (2004).
  - [9] W. von der Linden, *Physics Reports* **220**, 53 (1992).
  - [10] F. Verstraete, V. Murg, and J. I. Cirac, *Adv. Phys.* **57**, 143 (2008); G. Vidal, [arXiv:0912.1651](https://arxiv.org/abs/0912.1651) (2009); J. Haegeman, T. J. Osborne, and F. Verstraete, *Phys. Rev. B* **88**, 075133 (2013); R. Orus, *Ann. Phys.* **349**, 117 (2014).
  - [11] T. Sugihara, *J. High Energy Phys.* **2004**, 007 (2004).
  - [12] A. Milsted, J. Haegeman, and T. J. Osborne, *Phys. Rev. D* **88**, 085030 (2013).
  - [13] T. M. R. Byrnes, P. Sriganesh, R. J. Bursill, and C. J. Hamer, *Phys. Rev. D* **66**, 013002 (2002).
  - [14] M. C. Bañuls, K. Cichy, J. I. Cirac, and K. Jansen, *J. High Energy Phys.* **2013**, 1 (2013); M. C. Bañuls, K. Cichy, J. I. Cirac, K. Jansen, and H. Saito, in *PoS Lattice*, Vol. 332 (2013); M. C. Bañuls, K. Cichy, K. Jansen, and H. Saito, [arXiv:1603.05002](https://arxiv.org/abs/1603.05002) (2016).
  - [15] E. Rico, T. Pichler, M. Dalmonte, P. Zoller, and S. Montangero, *Phys. Rev. Lett.* **112**, 201601 (2014).
  - [16] B. Buyens, J. Haegeman, K. Van Acoleyen, H. Verschelde, and F. Verstraete, *Phys. Rev. Lett.* **113**, 091601 (2014); B. Buyens, J. Haegeman, H. Verschelde, F. Verstraete, and K. Van Acoleyen, [arXiv:1509.00246](https://arxiv.org/abs/1509.00246) (2015).
  - [17] S. Kühn, E. Zohar, J. I. Cirac, and M. C. Bañuls, *J. High Energy Phys.* **2015**, 1 (2015).
  - [18] T. Sugihara, *J. High Energy Phys.* **2005**, 022 (2005); in *AIP Conference Proceedings*, Vol. 756 (AIP Publishing, 2005) pp. 305–308.
  - [19] L. Tagliacozzo and G. Vidal, *Phys. Rev. B* **83**, 115127 (2011).
  - [20] P. Silvi, E. Rico, T. Calarco, and S. Montangero, *New J. Phys.* **16**, 103015 (2014).
  - [21] L. Tagliacozzo, A. Celi, and M. Lewenstein, *Phys. Rev. X* **4**, 041024 (2014).
  - [22] J. Haegeman, K. Van Acoleyen, N. Schuch, J. I. Cirac, and F. Verstraete, *Phys. Rev. X* **5**, 011024 (2015).
  - [23] A. Milsted and T. J. Osborne, “<https://github.com/tobiasosborne/lattice-gauge-theory-and-tensor-networks>,” (2015).
  - [24] M. Levin and C. P. Nave, *Phys. Rev. Lett.* **99**, 120601 (2007); Z.-C. Gu, F. Verstraete, and X.-G. Wen, [arXiv:1004.2563](https://arxiv.org/abs/1004.2563) (2010); Z.-C. Gu, *Phys. Rev. B* **88**, 115139 (2013).
  - [25] Y. Shimizu, *Mod. Phys. Lett. A* **27**, 1250035 (2012).
  - [26] Y. Shimizu and Y. Kuramashi, *Phys. Rev. D* **90**, 014508 (2014).
  - [27] J. F. Yu, Z. Y. Xie, Y. Meurice, Y. Liu, A. Denblyker, H. Zou, M. P. Qin, J. Chen, and T. Xiang, *Phys. Rev. E* **89**, 013308 (2014).
  - [28] J. Unmuth-Yockey, Y. Meurice, J. Osborn, and H. Zou,

- arXiv:1411.4213 (2014).
- [29] J. Kogut and L. Susskind, *Phys. Rev. D* **11**, 395 (1975).
- [30] S. Sachdev, *Quantum Phase Transitions*, 2nd ed. (Cambridge University Press, 2011).
- [31] J. M. Kosterlitz and D. J. Thouless, *J. Phys. C: Solid State Phys.* **6**, 1181 (1973).
- [32] P. Hasenfratz, M. Maggiore, and F. Niedermayer, *Physics Letters B* **245**, 522 (1990).
- [33] C. J. Hamer, J. B. Kogut, and L. Susskind, *Phys. Rev. D* **19**, 3091 (1979).
- [34] P. G. Hornby and M. N. Barber, *J. Phys. A: Math. Gen.* **18**, 827 (1985).
- [35] P. Butera and M. Comi, *Phys. Rev. B* **47**, 11969 (1993); P. Butera and M. Comi, *Phys. Rev. B* **54**, 15828 (1996).
- [36] G. Fox, R. Gupta, O. Martin, and S. Otto, *Nuclear Physics B* **205**, 188 (1982).
- [37] K. C. Wang and C. J. Hamer, *J. Phys. A: Math. Gen.* **26**, 5713 (1993).
- [38] P. Weisz, *Commun. Math. Phys.* **219**, 45 (2001).
- [39] F. Alet and E. S. Sørensen, *Phys. Rev. E* **67**, 015701 (2003).
- [40] H. H. Roomany and H. W. Wyld, *Phys. Rev. D* **21**, 3341 (1980).
- [41] J. Haegeman, B. Pirvu, D. J. Weir, J. I. Cirac, T. J. Osborne, H. Verschelde, and F. Verstraete, *Phys. Rev. B* **85**, 100408 (2012).
- [42] J. Haegeman, S. Michalakis, B. Nachtergaele, T. J. Osborne, N. Schuch, and F. Verstraete, *Phys. Rev. Lett.* **111**, 080401 (2013).
- [43] J. Shigemitsu and J. B. Kogut, *Nuclear Physics B* **190**, 365 (1981).
- [44] B. C. Hall, *Lie Groups, Lie Algebras, and Representations*, Graduate Texts in Mathematics, Vol. 222 (Springer International Publishing, Cham, 2015).
- [45] J. Haegeman, J. I. Cirac, T. J. Osborne, I. Pizorn, H. Verschelde, and F. Verstraete, *Phys. Rev. Lett.* **107**, 070601 (2011).
- [46] In particular, we use the operations provided by the CUBLAS library on NVIDIA Tesla K20 devices.
- [47] A. Milsted and M. Lewerenz, “<https://github.com/amilsted/evoMPS>,” (2015).
- [48] N. D. Mermin and H. Wagner, *Phys. Rev. Lett.* **17**, 1133 (1966); S. Coleman, *Commun. Math. Phys.* **31**, 259 (1973).
- [49] H.-L. Wang, J.-H. Zhao, B. Li, and H.-Q. Zhou, *J. Stat. Mech.* **2011**, L10001 (2011); D. Draxler, J. Haegeman, T. J. Osborne, V. Stojevic, L. Vanderstraeten, and F. Verstraete, *Phys. Rev. Lett.* **111**, 020402 (2013); V. Zauner, D. Draxler, L. Vanderstraeten, M. Degroote, J. Haegeman, M. M. Rams, V. Stojevic, N. Schuch, and F. Verstraete, *New J. Phys.* **17**, 053002 (2015).
- [50] C. R. Allton and C. J. Hamer, *J. Phys. A: Math. Gen.* **21**, 2417 (1988).
- [51] L. Tagliacozzo, T. R. de Oliveira, S. Iblisdir, and J. I. Latorre, *Phys. Rev. B* **78**, 024410 (2008).
- [52] V. Stojevic, J. Haegeman, I. P. McCulloch, L. Tagliacozzo, and F. Verstraete, *Phys. Rev. B* **91**, 035120 (2015).
- [53] P. Francesco, P. Mathieu, and D. Senechal, *Conformal Field Theory* (Springer Science & Business Media, 2012).
- [54] I. P. McCulloch and M. Gulácsi, *EPL* **57**, 852 (2002); S. Singh, R. N. C. Pfeifer, and G. Vidal, *Phys. Rev. A* **82**, 050301 (2010); A. Weichselbaum, *Ann. Phys.* **327**, 2972 (2012).